COMBINING EDGE-GRADIENT INFORMATION TO IMPROVE ADAPTIVE DISCONTINUITY-PRESERVING SMOOTHING OF MULTISPECTRAL IMAGES

George Lemeshewsky
U.S. Geological Survey
521 National Center
Reston, VA 22092
Open-File Report 94-252

ABSTRACT

A reported adaptive discontinuity-preserving smoothing technique was modified to improve the registration of interband edge features. With the unmodified technique, individual gray-scale images are convolved repeatedly with a small adaptive smoothing mask whose coefficients are a function of image gray-scale discontinuity, measured from edge gradients. After convergence, the image contains regions of uniform gray level separated by sharpened, steplike boundaries. However, adaptive smoothing of the individual bands of a multispectral image may cause relative displacements between corresponding sharpened steplike boundaries because of slight misregistrations and independent processing of each spectral band. In this study, a gradient-based adaptive smoothing technique was modified to include discontinuity information from all spectral band images. In contrast to independent smoothing, use of this modified technique aligns the interband boundaries. Several examples show adaptive smoothing of SPOT images for a three-band multispectral image and a combination of three multispectral and one panchromatic band images. In the latter, edge information from the higher resolution (10-m ground sample distance) panchromatic image somewhat improves the adaptive smoothing of the lower resolution (20-m ground sample distance) multispectral image. Preliminary results indicate that this modified adaptive smoothing technique improves the registration of edge boundaries between the multispectral image bands and may facilitate edge extraction

---

Any use of trade, product, or firm names is for descriptive purposes only and does not imply endorsement by the U.S. Government.

INTRODUCTION

Adaptive edge- or discontinuity-preserving smoothing is an image enhancement technique that preserves image edges while smoothing or generalizing other image regions (Pratt, 1978). Several adaptive smoothing techniques have been used for low-level processing of raw image data to enhance the subsequent extraction of edge and region features (Nagao and Matsuyama, 1979, and Chen and Medioni, 1992.)

Nagao and Matsuyama (1980) described adaptive edge-preserving smoothing (EPS) as a preprocessing technique for the segmentation of multispectral images, wherein each spectral band image was first smoothed to produce regions of constant intensity separated by sharpened, steplike edges. They observed boundary artifacts around larger uniform regions caused by slight misregistrations between the individual spectral band images and also by independently processing each image.

However, simple modifications to another type of adaptive smoothing technique can reduce the boundary and edge artifacts that may result from misregistrations and from the independent processing of multiband images. This report describes modifications to the adaptive discontinuity-preserving smoothing (DPS) technique described by Chen and Medioni (1992) and Saint-Marc and Chen (1991). These modifications incorporate edge discontinuity information from several multispectral band images to make sharpened boundaries coregister. Several preliminary examples of adaptive smoothing of SPOT (SPOT Image Corporation, 1988) images are given for (1) a 20-m ground sample distance (GSD), three-band multispectral (XS) image (interpolated to 10 m), and (2) the combination of XS and 10-m GSD panchromatic (P) images.

The latter example shows that the modified DPS technique creates sharpened edge boundaries in the lower resolution multispectral image that register with boundaries in higher resolution panchromatic images. Also there are examples that compare the EPS of Nagao and Matsuyama (1979, 1980) with the DPS of Chen and Medioni (1992).

METHODS

The calculations for DPS described by Chen and Medioni (1992) include the repeated convolution of an image with a small smoothing mask whose coefficients are determined adaptively from a measure of edge discontinuities within the image subregion defined by the mask. For this specific technique, discontinuities are measured from gradient magnitude data.

After many iterations and upon convergence, the image consists of regions of uniform amplitude, or gray level, separated by perfect steplike changes in gray level. Not only are small variations in gray level within regions smoothed, but image edges are sharpened as well. Also, they observed that edges were sharpened after a few iterations, but smoothing is extremely slow. This is advantageous because the sharpened edges can be detected readily with only simple edge-detection methods.

The unmodified adaptive smoothing technique for a single-band image involves the repeated convolution of an image with a 3- by 3-sample mask whose coefficients are a function of image discontinuities. Basically, these adaptive coefficients or smoothing weights will vary throughout the image as a function of image edge details in the subregion defined by the mask size. The larger the discontinuity, the smaller the smoothing coefficient and hence less smoothing of the discontinuity. In contrast, if the weights are fixed and equal, after many iterations all image discontinuities would be highly smoothed and eventually removed.

As Chen & Medioni (1992) describe, the smoothing weights at each iteration t for each image pixel location x, y are determined from a continuity value, $w_t(x, y)$, that is a decreasing function $f[\,.\,]$ of the discontinuity $d_t(x, y)$. That is

$$w_t(x, y) = f[\, d_t(x, y)\,] \tag{1}$$

where $f[\,0\,] = 1$ and $f[\, d_t(x, y)\,]$ approaches 0 as $d_t(x, y)$ increases. They used

$$w_t(x, y) = f[\, d_t(x, y)\,] = \exp(-|\, d_t(x, y)\,|^2 / 2k^2) \tag{2}$$

where

$$d_t(x, y) = [\, G_x^2(x, y) + G_y^2(x, y)\,]^{1/2} \tag{3}$$

is the magnitude of the gradient at x, y and

$$G_x(x, y) = 1/2(\, I_t(x + 1, y) - I_t(x - 1, y)\,) \tag{4}$$

$$G_y(x, y) = 1/2(\, I_t(x, y + 1) - I_t(x, y - 1)\,). \tag{5}$$

$G_x(x, y)$, $G_y(x, y)$ are the gradients at x, y and in the x and y axis directions, respectively; $I_t(x, y)$ is the adaptively smoothed image at iteration t. Parameter k functions like a threshold for the smoothing. If k is large, discontinuities will be removed; if small they will be preserved. Its value must be determined experimentally.

The smoothed image $I_{t+1}(x, y)$ at iteration $(t + 1)$ is given by Chen and Medioni (1992) as

$$I_{t+1}(x, y) = \frac{1}{N_t} \sum_{i=-1}^{+1} \sum_{j=-1}^{+1} I_t(x+i, y+j)\, w_t(x+i, y+j) \tag{6a}$$

where

$$N_t = \sum_{i=-1}^{+1} \sum_{j=-1}^{+1} w_t(x+i, y+j) \,. \tag{6b}$$

During the software implementation in this study, numerical underflow sometimes occurred with equation 2. To prevent this, the equation was modified as follows:

$$w_t(x, y) = f[\, d_t(\mathrm{x}, \mathrm{y})\,] = \exp(-|\, d_t(x, y)\,| / 2k^2). \tag{7}$$

That is, gradient magnitude, $|\, d_t(x, y)\,|$, replaced gradient magnitude squared, $|\, d_t(x, y)\,|^2$. Although equation 7 differs from equation 2, it still satisfies the properties described by Saint-Marc and Chen (1991); that is, $f[\, d_t(x, y)\,] = 1$ when $d_t(x, y) = 0$, and $f[\, d_t(x, y)\,]$ approaches 0 as $d_t(x, y)$ increases. Any differences in performance because of this change were believed to be minor and thus were not analyzed.

The DPS process is shown in figure 1 for image $I_t(x, y)$. Equations 3, 7, and 6 describe the calculations for boxes 1, 2, and 3, respectively. The symbol $|\nabla|$ denotes gradient magnitude.

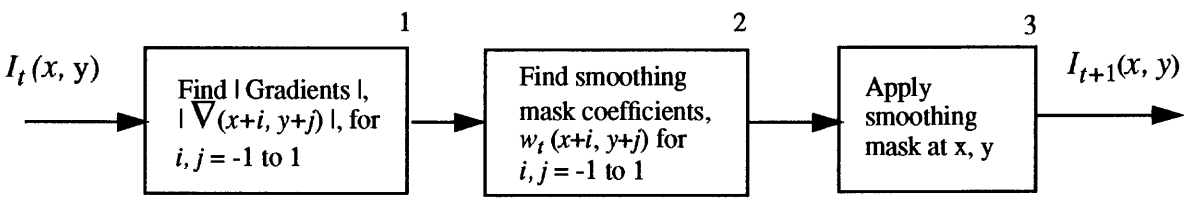

Figure 1. Adaptive discontinuity-preserving smoothing of image $I_t(x, y)$.

As the iterations, t, approach infinity, the process shown in figure 1 will produce steplike intensity discontinuities surrounding regions of near-constant intensity. It can be applied to the individual bands of multiband images.

Nagao and Matsuyama (1980) described an adaptive edge-preserving smoothing technique that also sharpens edges. Edge discontinuities were determined from statistical variance instead of from edge gradients. As noted earlier, they found that the location of the sharpened boundaries between uniform intensity regions of the individual multispectral images sometimes deviated because of slight misregistrations (about 1 pixel) between individual images and also because the bands were processed independently. Consequently, the image had many small boundary regions around larger regions. Additional processing (that is, region growing) was needed to remove these artificial boundaries (see Nagao and Matsuyama, 1980, for details).

MODIFIED DISCONTINUITY-PRESERVING SMOOTHING

In this study, the DPS technique of Chen and Medioni was modified so that edge gradients, a measure of edge discontinuities, were determined not only from the image subregion defined by the smoothing mask but also from several images. These edge data were combined to yield weights for one smoothing mask that was applied to each spectral band image.

Although the adaptive smoothing techniques of Nagao and Matsuyama or Chen and Medioni can be applied independently to multispectral image bands, the latter can be modified easily to incorporate edge information from all bands into the smoothing process for producing precisely registered and sharpened boundaries. As reported herein, figure 2 shows modified adaptive discontinuity-preserving smoothing, DPS-M, in which the smoothing coefficients are determined from the gradients of several image bands

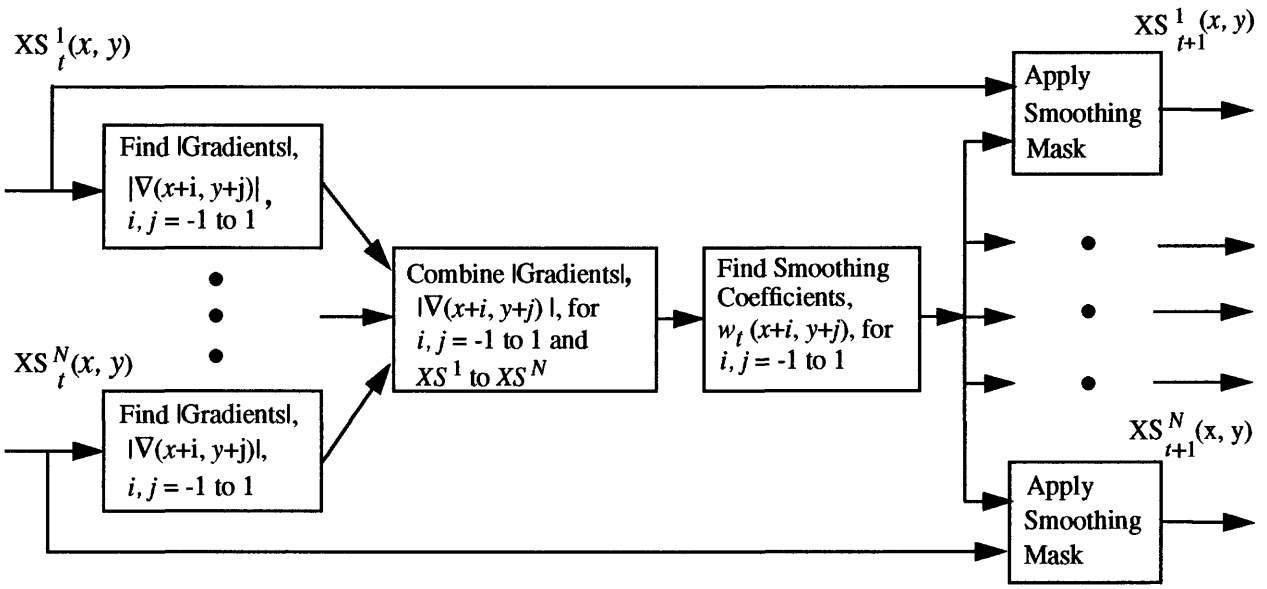

Figure 2. Modified adaptive discontinuity-preserving smoothing for multiband images.

Here one set of smoothing coefficients, derived from the *combined* gradient information, is applied to each multispectral band image, XS^k, $k = 1$ to N. As in figure 1, for each box labeled "Find |Gradients|," nine gradient magnitudes are calculated for the small 3- by 3-pixel region

around image pixel location x, y, and for each iteration, t. The remaining calculations, "Find Smoothing Coefficients" and "Apply Smoothing Mask," are the same as in figure 1.

For each iteration t and image pixel location (x, y), the combined gradient magnitude, $|\nabla'(x+i, y+j)|$, was calculated from nine gradient magnitudes for each image XS^k, where $k = 1$ to N, as

$$|\nabla'(x+i, y+j)| = \text{MAX} \left[|\nabla^{XS^1}(x+i, y+j)|, |\nabla^{XS^2}(x+i, y+j)|, \ldots |\nabla^{XS^N}(x+i, y+j)| \right] \quad (8)$$

and for $i, j = -1$ to 1. $|\nabla(x, y)|$ was given by equation 3.

The new gradient magnitude is a measure of the maximum gradient in all bands. Because the smoothing mask coefficients vary inversely with the gradient magnitude, as in equation 7, large edges generate relatively small smoothing mask coefficients. Thus, large edge amplitudes in one band may prevent excessive smoothing of smaller edge features in other bands. Also, because only one adaptive smoothing mask is applied to all images, later examples will show that the resulting steplike boundaries in the individual images have improved coregistration.

In equation 8, all gradient magnitudes $|\nabla|$ have equal weight; that is, no preference is given to any one image. However, weighting factors could readily be incorporated into the gradient magnitude integration of equation 8. For example, gradient magnitude information between two images might be combined as

$$|\nabla'(x+i, y+j) = \alpha |\nabla^{XS^1}(x, y)| + (1 - \alpha) |\nabla^{XS^2}(x, y)| \quad (9)$$

where constant α, $0 \leq \alpha \leq 1$, controls the degree of integration between gradient information of images XS^1 and XS^2 and $i, j = -1$ to 1. However, preliminary tests, not described here, indicated that the MAX function of equation 8, rather than the weighting of equation 9, prevented excessive smoothing of smaller amplitude edges. This is a subject of further study.

EXAMPLES

In all the following examples, the 128- by 128-pixel test image was from a four-band SPOT scene, (processing level 1b) consisting of one panchromatic band (P) with 10-m GSD and three multispectral (XS) bands, (XS1, XS2, XS3), with 20-m GSD. This scene has been registered to a universal transverse mercator coordinate system by means of ground control points and coordinate system transformation; all image bands have been cubic interpolated to 10-m ground sample distance. Although the band-to-band displacement error in the sample image is relatively large, about $\pm$ 1 pixel, no attempt was made to reduce this error. In fact, this displacement helps to illustrate the displaced and sharpened boundaries after adaptive smoothing.

Figure 3 shows a plot of gray-level value versus sample distance along a row of the four-band SPOT image sample. Here sample 0 begins at row 40, column 10 relative to the image's upper left corner.

Figures 4 and 5 show the result of 10 iterations of EPS and DPS (without gradient integration) for the XS image. In both figures the edge boundaries have been sharpened while other regions have been smoothed to near-constant levels. Ultimately, additional iterations produce perfect step edges and regions of constant intensity. Also note that many edges do not align.

In this and all subsequent examples of EPS or DPS, 10 iterations were performed, and parameter k of equation 7 was 1.0 for DPS. Earlier tests determined that $k = 1.0$ prevented excessive smoothing of small amplitude edges.

Figure 6 shows the result of DPS modified with gradient integration (DPS-M) applied to the XS image. In contrast to the previous plots of figures 4 and 5, notice that the sharpened, step-like edges (for example at sample 37) now are nearly coincident with the edge having the highest gradient magnitude.

Images in the following three figures (7, 8, and 9) illustrate EPS or DPS with or without gradient integration for the XS or the combination XS and P images. To enhance the visibility of minor variations in color, and where noted, the XS image, normally displayed here as XS3 to red, XS1 to green, and XS2 to blue, was transformed to intensity (I), hue (H), and lightness (L) (IHL) (Adobe, 1991) and then displayed as red, green, and blue, respectively. However, all XS edge illustrations were done by means of a Sobel edge enhancement (Adobe, 1991) of the three XS bands, not the IHL image. They show raw edge data without thresholding or thinning (Pratt, 1978).

Figure 7 compares EPS and DPS without gradient integration of an XS image. As noted above, several images are displayed as IHL. Relative displacements between sharpened edge boundaries are visible in the edge-enhanced images, (e) and (f), and also as long narrow features in (c) and (d).

Figure 8 shows DPS with gradient integration for the following three test conditions: (1) DPS, gradient integration on three XS bands, (2) DPS, gradient integration on four bands (XS1, XS2, XS3, and P), and (3) DPS of the P image. The adaptive DPS, modified with gradient integration, on three XS bands can be compared with DPS, no gradient integration, as figure 8, (d), (g), and (j) and figure 7, (d), (f), and (h).

Figure 8 (e), (h), and (k) shows XS image results for DPS when gradient information was combined from three SPOT XS bands *and* one P band. Figure 8 (c), (f), and (i) shows respectively, P image, DPS P image, and Sobel-enhanced edges.

Because the sharpened edges are no longer displaced in these examples, there are no narrow borders around larger regions of figure 8 (d) or (e), as compared with figure 7 (d). Similarly, the enhanced edges of figure 10 (j) or (k) are distinct, narrow, and coincident.

For clarity, image (i), the enhanced edges of (f), is repeated as (l). Comparing edges of figures 10 (j), (k), and (i), note that some additional spatial detail (for example the small square borders) from the 10-m GSD P image appears in (k); (k) is a result of DPS with four-band (XS1, XS2, XS3, and P) gradient integration.

In figure 9, image (c) shows the XS image after adaptive smoothing (as in figure 2, 10 iterations, k=1.0), with gradient integration derived from four image bands: three multispectral bands and one panchromatic band. Image (d) is the result of independently adaptive smoothing each XS band as in figure 1. The shadowlike borders in (d) are a consequence of this independent processing. In contrast, (c) has the desired sharp, distinct boundaries around the regions of uniform color because of the improved registration of the corresponding boundaries in each respective band.

CONCLUSIONS

Several examples showed that two adaptive smoothing techniques, when applied independently to the individual bands of a multispectral image, can lead to displacements between the resulting sharpened, steplike edges. Such displacements appear as small artificial boundaries around larger smoothed regions.

Modifications were made to an adaptive smoothing technique to combine edge gradients from multiple image bands. Several examples of this modified smoothing, including edge profile plots and images, showed that sharpened edge boundaries coincide and artificial boundaries around larger regions are eliminated. Also, in one example edge detail from a higher spatial resolution (10-m GSD) panchromatic image was integrated into the adaptively smoothed, lower spatial resolution (GSD 20-m) XS image.

The improved boundary registration that is due to gradient modified adaptive smoothing should facilitate subsequent edge and region segmentation in multispectral images.

REFERENCES

Adobe Systems Inc., 1991, Adobe photoshop users guide: Mountain View, Calif.

Chen, J.S. and Medioni, G., 1992, Adaptive smoothing: principles and applications, chap. 1 *of* Mahdavieh, Y. and Gonzalez, R.C., eds., Advances in image analysis: Bellingham, Wash., SPIE, p. 13-51.

Nagao, M., and Matsuyama, T., 1980, Some basic techniques in picture processing and feature extraction, chap. 3 and Extraction of characteristic regions, chap. 5 *of* A structured analysis of complex aerial photographs: New York, Plenum Press, p. 32-82 and p. 98-118.

Nagao, M., and Matsuyama, T., 1979, Edge preserving smoothing: Computer Vision, Graphics and Image Processing, v. 9, p. 394-407.

Pratt, W. K., 1978, Image feature extraction, chap. 17 *of* Digital image processing: New York, Wiley, p. 471-513.

Saint-Marc, P., and Chen, J.S., 1991, Adaptive smoothing: A general tool for early vision: IEEE Trans. Pattern Analysis And Machine Intelligence, v. 13, p. 514-529.

SPOT Image Corporation, 1988, SPOT user's handbook: Reston, Va., v. 2, chap. 1.

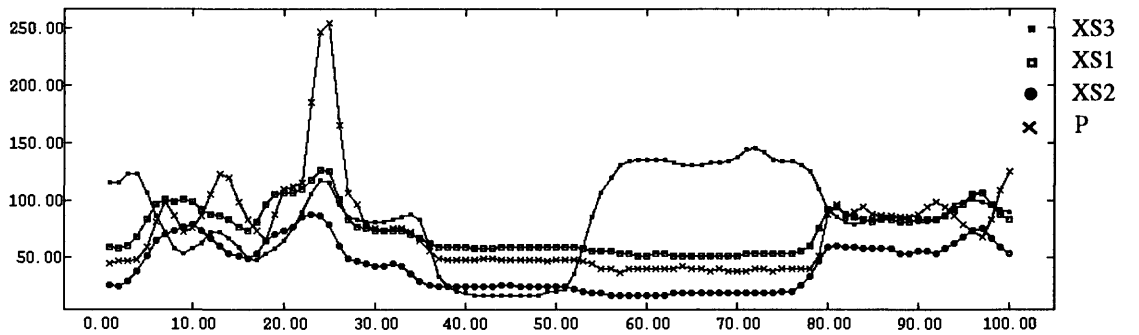

Figure 3. Pixel gray-level profile for panchromatic (P) and three multispectral (XS) band images.

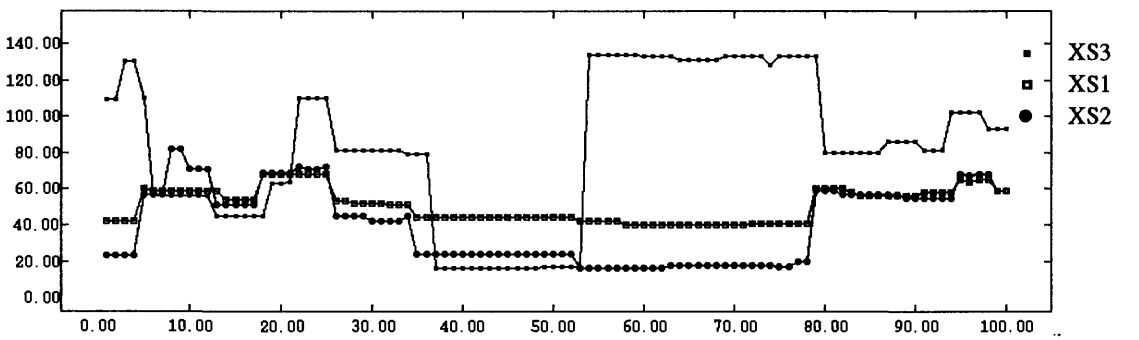

Figure 4. XS data after 10 iterations of edge-preserving smoothing (EPS).

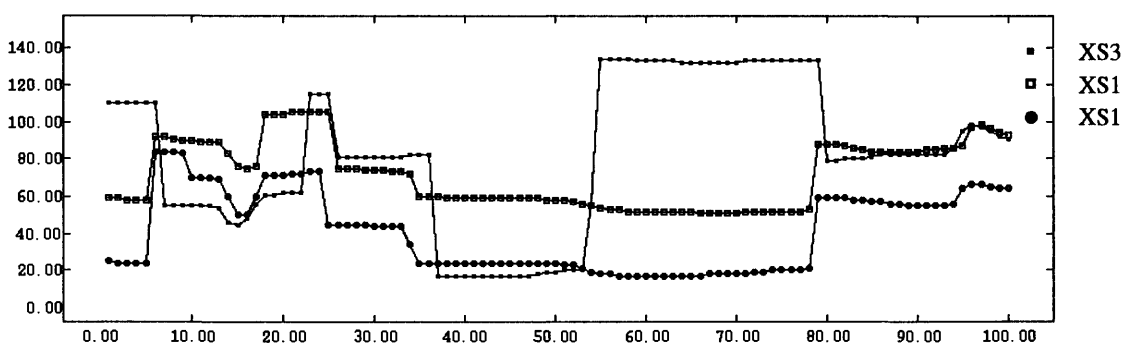

Figure 5. XS data after 10 iterations of discontinuity-preserving smoothing (DPS); no gradient integration.

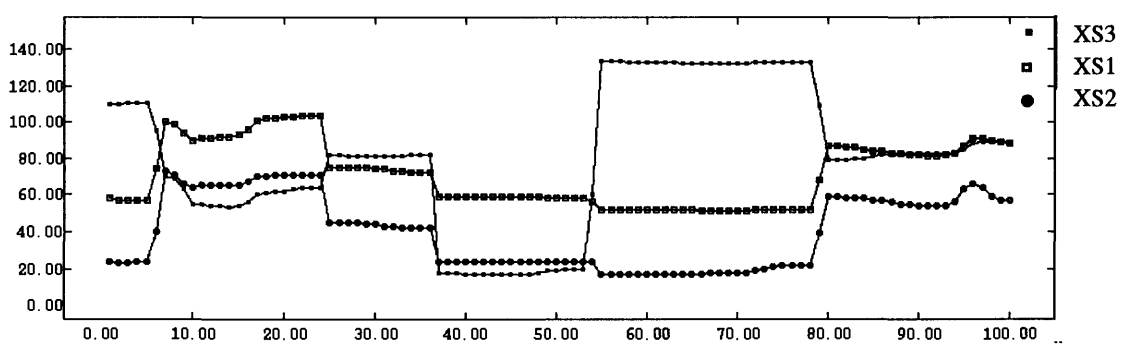

Figure 6. XS data after 10 iterations of DPS; with gradient integration. Note here, as compared to figure 4, that the sharpened, steplike edges are now registered.

a

b

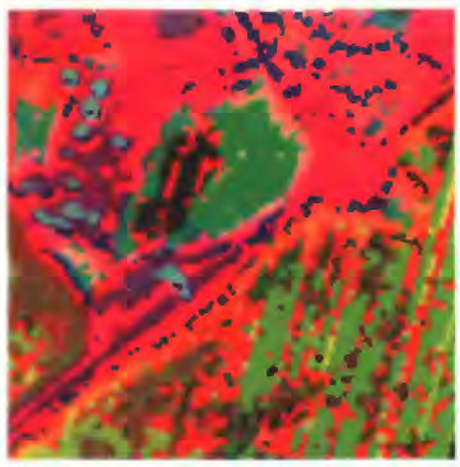

(a) XS Image

(b) XS image (a) as IHS

c

d

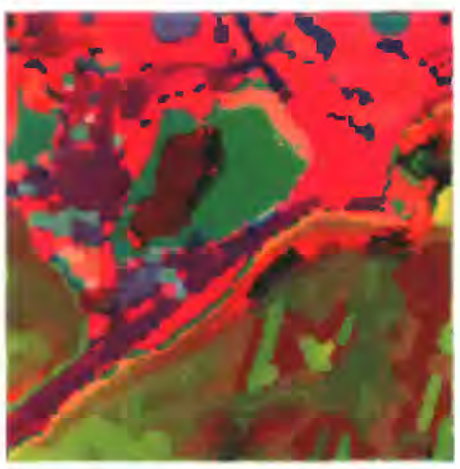

(c) edge-preserving smoothing, EPS, of (a); displayed as IHL.

(d) discontinuity-preserving smoothing (figure 1), DPS, of (a); displayed as IHL.

e

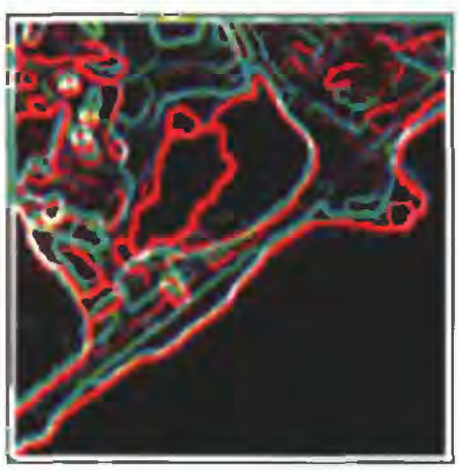

f

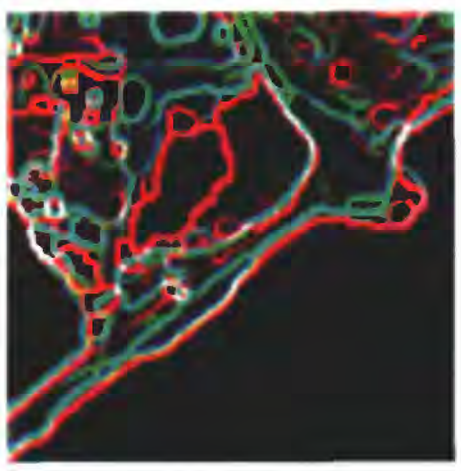

(e) Sobel-enhanced edges of (c); however, derived from XS as R, G, and B, not IHL.

(f) Sobel-enhanced edges of (d); however, derived from XS as R, G, and B, not IHL.

g

h

(g) Intensity, (that is, average R,G and B) of (e).

(h) Intensity, (that is, average R, G and B) of (f).

Figure 7. Adaptive smoothing (AS) of three-band multispectral (XS) image.

(a) SPOT XS image bands XS3, XS1, and XS2 displayed as red (R), green (G), and blue (B). (b) is image (a) after color enhancement by means of transforming to intensity, hue, and lightness (IHL), and displayed as R, G, and B, respectively. (c) through (h) show effects of displaced, sharpened boundaries caused by AS of each band independently: artificial borders, (c), (d), around larger regions and nonregistered edge boundaries, (e), (f), (g), and (h). All Sobel-enhanced edge data were from the smoothed XS3, XS1, XS2 band images.

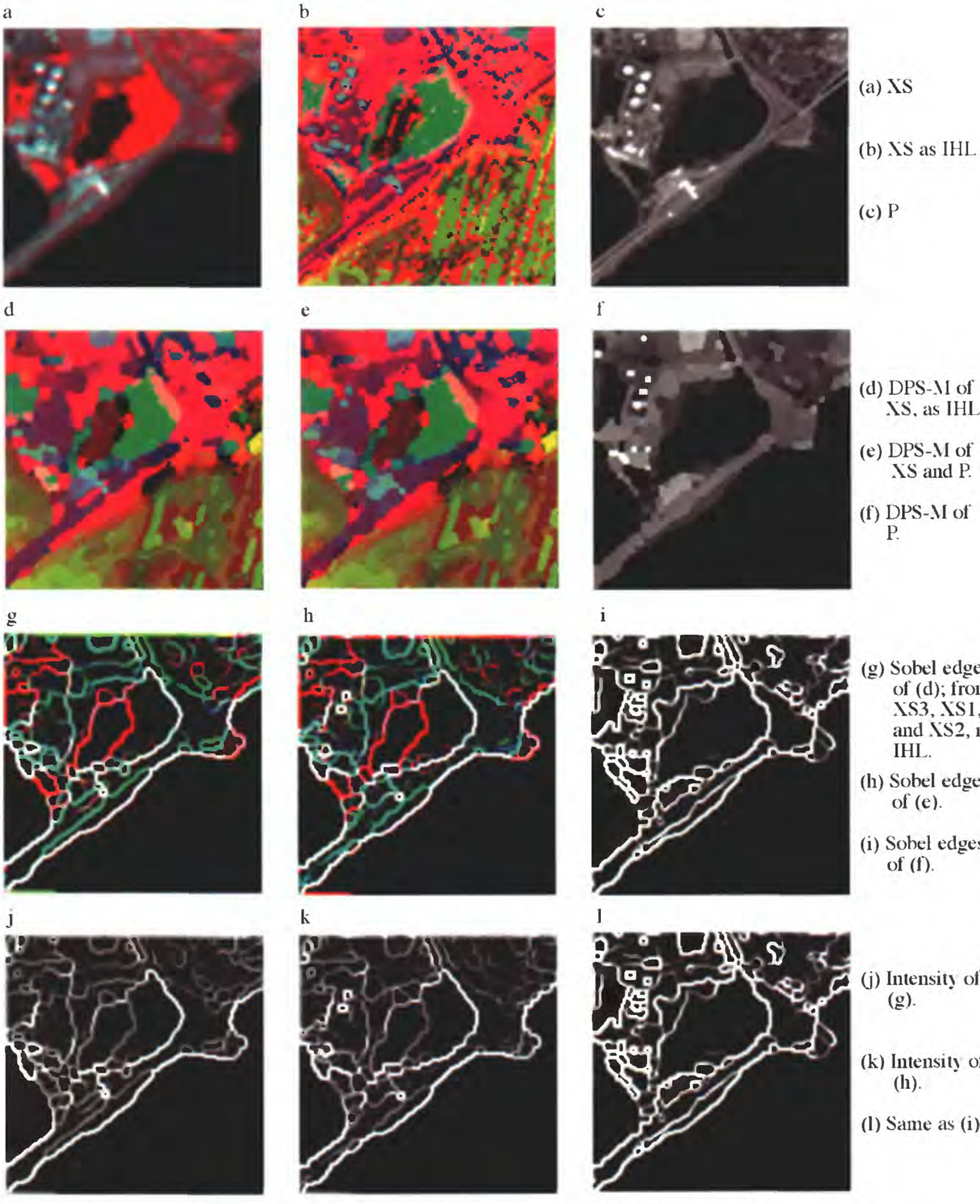

Figure 8. Discontinuity-preserving smoothing, modified with gradient integration, DPS-M.

These images illustrate DPS-M of a multispectral image, XS, when gradient information was integrated from: 1. the three XS bands or 2. three XS bands plus one panchromatic band, P. Also, as in figure 7, the XS images were transformed to IHL. All Sobel-enhanced XS edge data were from the smoothed XS3, XS1, and XS2 band images. Note in (d) or (e), compared to (c) or (d) of figure 7, the absence of artificial border regions. In (g), (h), and (j), compared to figure 7 (e) to (h), the edges are not displaced. Comparing (j), (k), and (l), observe that (k) also includes spatial detail from the P image.

a

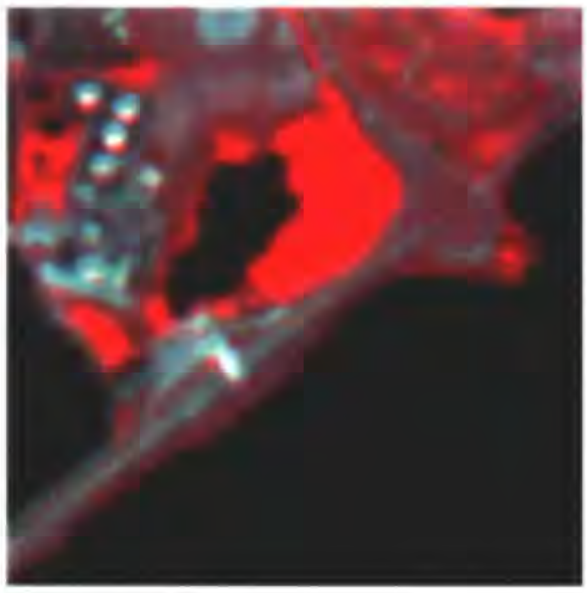

b

c

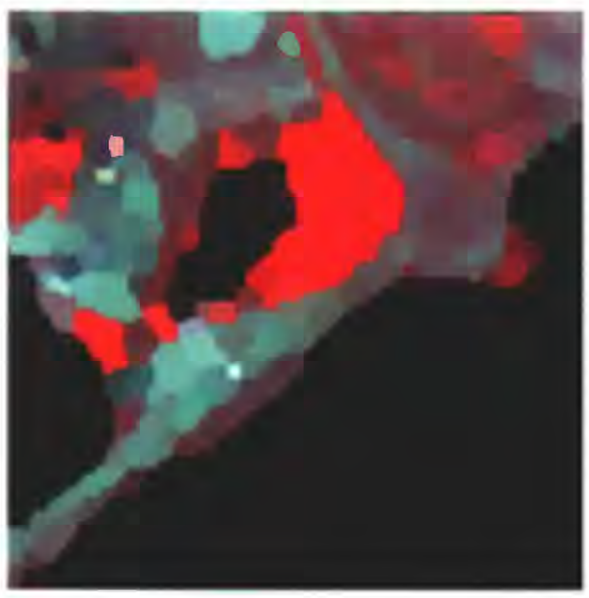

d

Figure 9. Adaptive smoothing with and without multiband gradient integration.

Image (c) shows adaptive smoothing (10 iterations) with gradient integration (that is, figure 2) of four bands: the three multispectral bands of image (a) and the panchromatic band of image (b). (d) is the result of independent adaptive smoothing (that is, figure 1) of each XS band of (a). In (d), the shadowlike borders are a consequence of this independent processing. In contrast, note in (c) the desired sharp, distinct boundaries around the regions of uniform color caused by the improved registration of the corresponding boundaries in each respective band.